

Multifunctional Core–Shell Silica Nanoparticles for Highly Sensitive ^{19}F Magnetic Resonance Imaging**

Hisashi Matsushita, Shin Mizukami, Fuminori Sugihara, Yosuke Nakanishi, Yoshichika Yoshioka, and Kazuya Kikuchi*

Abstract: ^{19}F magnetic resonance imaging (^{19}F MRI) is useful for monitoring particular signals from biological samples, cells, and target tissues, because background signals are missing in animal bodies. Therefore, highly sensitive ^{19}F MRI contrast agents are in great demand for their practical applications. However, we have faced the following challenges: 1) increasing the number of fluorine atoms decreases the solubility of the molecular probes, and 2) the restriction of the molecular mobility attenuates the ^{19}F MRI signals. Herein, we developed novel multifunctional core–shell nanoparticles to solve these issues. They are composed of a core micelle filled with liquid perfluorocarbon and a robust silica shell. These core–shell nanoparticles have superior properties such as high sensitivity, modifiability of the surface, biocompatibility, and sufficient *in vivo* stability. By the adequate surface modifications, gene expression in living cells and tumor tissue in living mice were successfully detected by ^{19}F MRI.

Magnetic resonance imaging (MRI) can provide valuable information about deep tissues in animal bodies with high spatial resolution without using radioactivity. ^{19}F MRI is an especially powerful method for *in vivo* imaging of particular biomolecules, cells, and target tissues, because of negligible background signals.^[1] In ^{19}F MRI, fluorinated agents need to

be delivered with high density per voxel to give signals of sufficient intensity.^[2] Thus, highly sensitive ^{19}F MRI probes are required for their practical applications. To addressing this sensitivity problem, it is important to increase the number of fluorine atoms in the MRI probes. However, simple multiplication of the fluorine atoms does not provide higher sensitivity because of the following two reasons: 1) increasing the number of fluorine atoms decreases the solubility of the molecular probes^[3] and 2) suppression of the molecular mobility induced by the increase in the molecular size shortens the transverse relaxation time (T_2), resulting in attenuation of the MRI signal.^[4] To solve these two problems simultaneously, we designed a novel ^{19}F MRI probe consisting of a core–shell nanoparticle that involves a perfluoro-[15] crown-5 ether (PFCE).

PFCE has various attractive characteristics as a ^{19}F MRI contrast agent. First, PFCE has 20 equivalent fluorine atoms, which show a sharp single ^{19}F NMR peak to yield a strong signal. Second, a large number of liquid PFCE are expected to maintain their high molecular mobility in a nanoparticle. Taking these advantages, PFCE nanoemulsions have been reported for *in vivo* cell tracking.^[5] However, the instability of PFCE nanoemulsions in organic solvents significantly limits their application through surface modifications. Even under neutral buffer conditions, Ostwald ripening, which is a molecular diffusion phenomenon resulting in the gradual growth of larger particles, can be a major problem for the stability.^[6] To overcome this limitation, we considered to cover the PFCE nanoemulsion with a silica shell (Figure 1 a). Silica nanoparticles possess attractive features such as biological inertness and favorable colloidal properties.^[7] In addition, the silica surface can be variously modified with functional groups to realize the targeted delivery and specific functions. Herein, we report a novel multifunctional ^{19}F MRI contrast agent, fluorine accumulated silica nanoparticle for MRI contrast enhancement (FLAME), and demonstrate the superior properties for ^{19}F MRI such as high sensitivity, stability, modifiability of the surface, biocompatibility, and biomedical applications such as reporter assay and *in vivo* tumor imaging.

The synthetic protocol of FLAME is presented in Figure 1 b. To cover the PFCE-phospholipid nanoemulsion with silica gel, we developed a novel surfactant, PAP (Scheme S1), which consists of an alkyl part to interact with phospholipids^[8] and a basic pyridinyl group. When template nanoemulsions are formed in the presence of PAP, the basic site of PAP was expected to be displayed on the nanoemulsion surface and to initiate the sol–gel process of tetraethyl orthosilicate.^[9] As a result, the silica polymerization reaction occurred only near the nanoemulsion surface, and silica coating of the PFCE

[*] H. Matsushita, Dr. S. Mizukami, Y. Nakanishi, Prof. K. Kikuchi
Graduate School of Engineering, Osaka University
Osaka 565-0871 (Japan)
E-mail: kkikuchi@mls.eng.osaka-u.ac.jp
Homepage: <http://www-molpro.mls.eng.osaka-u.ac.jp/English/indexeng/indexENG.html>

Dr. F. Sugihara, Prof. Y. Yoshioka
Immunology Frontier Research Center
Osaka University, Osaka 565-0871 (Japan)

[**] This research was supported by the Ministry of Education, Culture, Sports, Science, and Technology (Japan) (grant numbers 24108724, 24685028, 24115513, 24651259, 25620133, and 25220207), by the Japanese Society for the Promotion of Science (JSPS) through its Funding Program for World-Leading Innovative R&D on Science and Technology (FIRST Program), and by CREST from JST. The authors acknowledge the Asahi Glass Foundation and the Magnetic Health Science Foundation. The authors thank Prof. Tsutomu Ono (Okayama University) for helpful discussion to synthesize nanomaterials, and Dr. Takayuki Kato and Dr. Takao Sakata (Osaka University) for their support in TEM measurements. Some of the experiments were carried out at the Research Center for Ultra-High Voltage Electron Microscopy, Osaka University. The authors also thank Dr. Yuko Kamikawa (Osaka University) for the valuable discussion.



Supporting information for this article is available on the WWW under <http://dx.doi.org/10.1002/anie.201308500>.

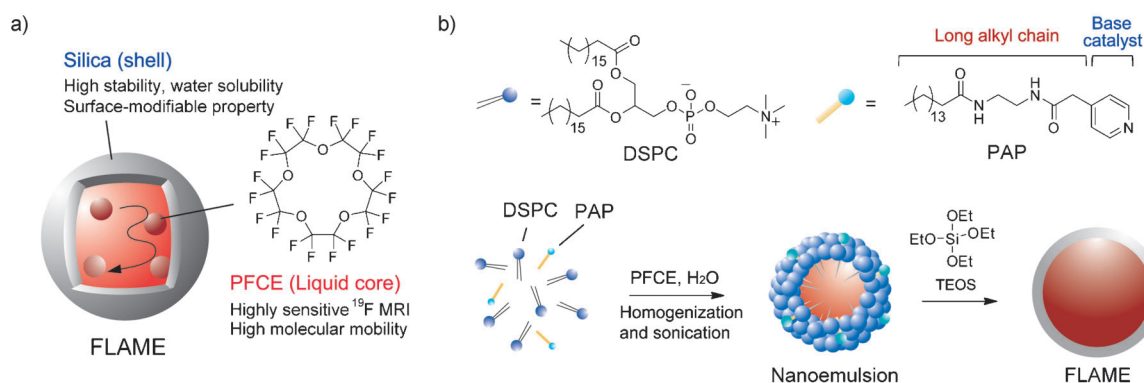


Figure 1. Design and synthetic strategy of FLAME. a) The components of FLAME. b) The chemical structure of PAP and synthesis of FLAME.

nanoemulsion was achieved (Scheme S2). Rhodamine B isothiocyanate (RITC) was covalently attached to the silica shell, which allowed for the fluorescence detection.

The core-shell structures of FLAME were clearly observed by transmission electron microscopy (TEM; Figure 2a). The average diameter of the particles was 76 ± 9 nm

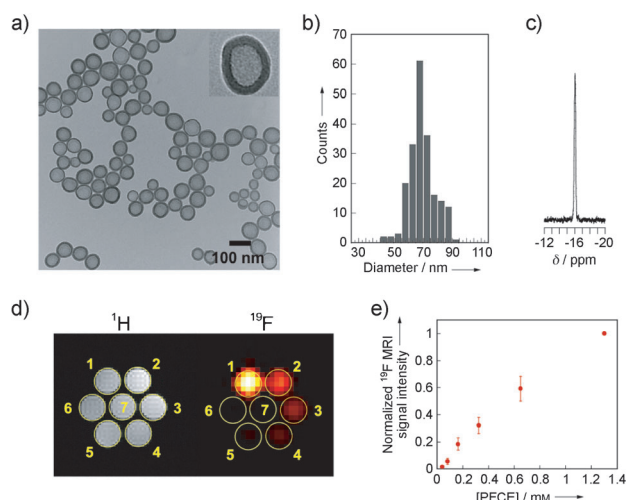


Figure 2. Characterization of FLAME. a) TEM image of FLAME. b) Particle size distribution histogram calculated from TEM images. c) ^{19}F NMR spectrum of FLAME in PBS (pH 7.4). d) MRI of phantoms (1–6) filled with FLAME in PBS (500 μL). PFCE concentrations: 1.30, 0.650, 0.325, 0.163, 0.0813, and 0.0406 mm for phantoms 1–6, respectively. Phantom 7 contains PBS. e) Plot of the normalized ^{19}F MRI signal intensity versus PFCE concentration.

(Figure 2b). On the other hand, the silica shell was not well formed in the absence of PAP (see Figure S1 in the Supporting Information). Dynamic light scattering (DLS) measurements also indicated the silica coating of nanoemulsion. The hydrodynamic diameter was changed from 80 nm of the nanoemulsion to 131 nm of FLAME, and the ζ potential decreased from +29.5 mV of the nanoemulsion to -4.5 mV of FLAME (Figure S2 and Table S1). Inclusion of PFCE in the particle was confirmed by NMR spectroscopy. The ^{19}F NMR spectroscopy of FLAME dispersed in phosphate-buffered saline (PBS) solution showed a PFCE-derived single peak at

-16.4 ppm (Figure 2c). In the ^{19}F MRI measurements, strong ^{19}F MRI signals were observed from FLAME (Figure 2d). The ^{19}F MRI signal intensity was proportional to the PFCE concentration (Figure 2e). FLAME showed the typical fluorescence emission of RITC (Figure S3).

To demonstrate the high ^{19}F MRI sensitivity, FLAME was applied to a ^{19}F MRI-based reporter assay. We chose a BL-tag protein as a reporter protein,^[10] which is a noncatalytic β -lactamase mutant that covalently binds various β -lactam structures. Thus, ampicillin-modified FLAME (FLAME-Amp) was prepared for the specific ^{19}F MRI detection of the reporter protein (Figure 3a, Scheme S3, and Table S1). To confirm the specific binding of FLAME-Amp to the BL-tag protein, we used a fusion protein of BL-tag and maltose-binding protein (MBP), which noncovalently bind to an amylose with high affinity (Scheme S4). After FLAME-Amp was incubated with an MBP-BL-bound amylose resin, the nonbound components were removed by washing with a buffer solution (Figure S4). Then, the fractions eluted with a maltose solution were analyzed by ^{19}F NMR spectroscopy. A sufficiently high and sharp ^{19}F NMR peak was detected from MBP-BL incubated with FLAME-Amp (Figure 3b). The ^{19}F NMR peak was detected even at a MBP concentration of 30 nM.

A small molecule-based probe, F-Amp, was also synthesized to evaluate the ^{19}F MRI sensitivity (Scheme S5 and Figure S5). The ^{19}F NMR signal of F-Amp was not observed at a MBP-BL concentration of 300 nM. At least concentrations of the target protein in the micromolar range were required for NMR detection by the small-molecule probe because of the low ^{19}F density per probe. In contrast, FLAME-Amp encapsulating a large amount of fluorine atoms enabled the detection of the target proteins in the nanomolar range (Figure S6 and Table S2). Another important factor for sensitivity improvement is the rotational mobility of fluorine atoms. The mobility of small-molecule probes is largely decreased by the binding to proteins; furthermore, it causes the T_2 reduction, which decreases the NMR signal. The T_2 of F-Amp drastically shortened from 0.434 s to 0.119 s by the covalent binding to MBP-BL and the ^{19}F NMR signal was decreased (Figure S7). On the other hand, the T_2 of FLAME-Amp conjugated to MBP-BL was 0.210 s, which is comparable to that of FLAME-Amp (0.238 s;

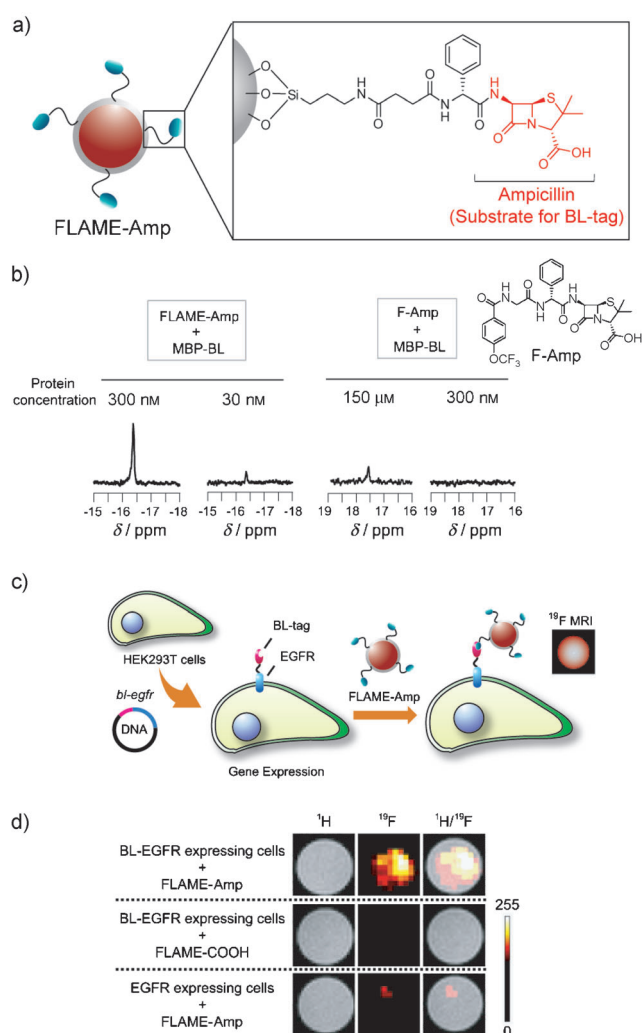


Figure 3. ¹⁹F NMR/MRI detection of BL-tag protein. a) The chemical structure of FLAME-Amp. b) Highly sensitive ¹⁹F NMR detection of MBP-BL proteins with FLAME-Amp. c) ¹⁹F MRI detection of gene expression using BL-EGFR and FLAME. d) MRI of BL-EGFR-expressing HEK293T cells treated with FLAME-Amp, FLAME-COOH, and EGFR-expressing cells treated with FLAME-Amp.

Table S3). These results demonstrate that the rotational motion of PFCE was maintained even after FLAME was attached to a protein.

Next, ¹⁹F MRI detection of gene expression was attempted using a cell surface-displayed reporter protein (Figure 3c). In this experiment, the BL-tag was fused to the epidermal growth factor receptor (EGFR), which is a membrane-associated glycoprotein,^[11] the recombinant protein was expressed on the surface of HEK293T cells.^[10] After FLAME-Amp was incubated with cells expressing BL-EGFR, MRI experiments were performed. The strong ¹⁹F MRI signal was clearly observed from BL-EGFR-expressing cells incubated with FLAME-Amp, whereas almost no signal was detected from the control EGFR-expressing cells (Figure 3d and Figure S8). As a result, specific and highly sensitive ¹⁹F MRI detection of gene expression in living cells was successfully demonstrated by FLAME-Amp.

Finally, the potential of FLAMEs for in vivo targeting were evaluated in tumor-bearing mice. The nanomaterials were delivered to the tumor using the enhanced permeability and retention (EPR) effect, which promotes nanoparticle accumulation in cancerous tissues by a combination of leaky angiogenic blood vessels and deficient tumor lymphatics.^[12]

However, the naked nanoparticles should be trapped immediately by the reticuloendothelial system (RES) and show a decreased circulation time. Therefore, FLAME was modified with polyethylene glycol (PEG) for the effective delivery to tumors (Figure 4a). PEGylation reduces the uptake by increasing the electrostatic interactions with proteins and small molecules.^[13]

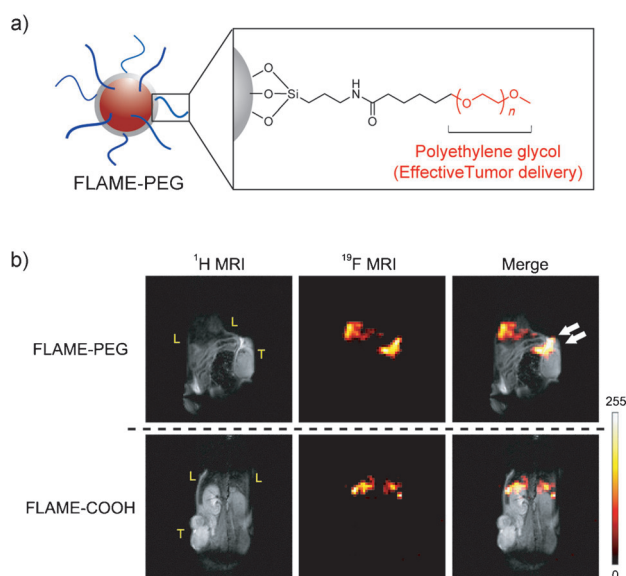


Figure 4. In vivo accumulation of FLAME at tumor site. a) Structure of FLAME-PEG and FLAME-COOH b) In vivo MRI of FLAME-PEG and FLAME-COOH in tumor-bearing mice. The positions of the liver and tumor are represented as L and T, respectively.

PEGylated FLAME (FLAME-PEG) was synthesized from FLAME-NH₂ (Scheme S6 and Table S1). DLS analysis to determine the stability of FLAME-PEG showed that there was almost no change in the particle size for 1 week (Figure S9). The biocompatibility of FLAME-PEG was evaluated in the MTT assay. The viability of colon-26 cells was not affected by 24 h exposure of FLAME-PEG and up to 900 μg mL⁻¹ of PFCE (Figure S10).

Passive targeting and accumulation of FLAME-PEG using the EPR effect were demonstrated by MRI. Mice bearing a tumor were given intravenous injections of FLAMEs (Figure 4b). Strong ¹⁹F MRI signals of FLAME-PEG at the tumor site indicated passive targeting of the nanoparticles. The ¹⁹F NMR measurements of homogenized tissue samples showed that NMR signals were detected only from liver ($C_{\text{PFCE}} = 113 \text{ nmol g}^{-1}$) and tumor ($C_{\text{PFCE}} = 28.8 \text{ nmol g}^{-1}$), but not from spleen, lungs, brain, kidneys, and heart (Figure S11). However, the ¹⁹F MRI signals of non-PEGylated FLAME-COOH (Scheme S3) was detected only in the liver, indicating that FLAME-COOH was immediately

trapped by the RES. These results indicate that the ^{19}F MRI signals of FLAMEs are sufficiently strong for in vivo studies. The accumulation of FLAME-PEG in tumor and liver sections was verified by the RITC fluorescence (Figure S12). Meanwhile, in the case of FLAME-COOH, fluorescence signals were detected only in the livers and spleens, not at the tumors (Figure S13). These results demonstrate that the ^{19}F MRI signal localization reflects the actual accumulation position of FLAMEs in animal bodies.

In conclusion, we have successfully developed novel contrast agents with a core-shell structure, FLAMEs, for highly sensitive ^{19}F MRI. By coating the surface with silica, FLAMEs demonstrated practical properties such as a chemically modifiable surface, dispersibility in water, biocompatibility, and high stability. FLAMEs were proven to be useful ^{19}F MRI contrast agents to overcome two major limitations of current ^{19}F MRI probes, that is, an impractical modifiability of the surface of nanoemulsions and a low sensitivity of small-molecule-based probes. As an extension of the ^{19}F MRI-based reporter assay shown in this study, in vivo evaluation of gene transplantation efficiency is one of the promising future applications. FLAME could also lead to various biomedical applications such as ^{19}F MRI of atherosclerosis plaques with a clot-binding peptide^[14] or bone neoplasms with bisphosphonate.^[15]

Received: September 30, 2013

Keywords: fluorine · imaging agents · magnetic resonance imaging · nanoparticles

- [1] a) M. Higuchi, N. Iwata, Y. Matsuba, K. Sato, K. Sasamoto, T. C. Saïdo, *Nat. Neurosci.* **2005**, *8*, 527–533; b) S. Mizukami, R. Takikawa, F. Sugihara, Y. Hori, H. Tochio, M. Wälchli, M. Shirakawa, K. Kikuchi, *J. Am. Chem. Soc.* **2008**, *130*, 794–795; c) Y. Takaoka, T. Sakamoto, S. Tsukiji, M. Narazaki, T. Matsuda, H. Tochio, M. Shirakawa, I. Hamachi, *Nat. Chem.* **2009**, *1*, 557–561; d) M. Srinivas, A. Heerschap, E. T. Ahrens, C. G. Figdor, I. J. M. de Vries, *Trends Biotechnol.* **2010**, *28*, 363–370.
- [2] J. Ruiz-Cabello, B. P. Barnett, P. A. Bottomley, J. W. M. Bulte, *NMR Biomed.* **2011**, *24*, 114–129.
- [3] J. Liu, L. S. Lee, *Environ. Sci. Technol.* **2007**, *41*, 5357–5362.
- [4] K. Tanaka, N. Kitamura, K. Naka, Y. Chujo, *Chem. Commun.* **2008**, 6176–6178.
- [5] E. T. Ahrens, R. Flores, H. Xu, P. A. Morel, *Nat. Biotechnol.* **2005**, *23*, 983–987.
- [6] a) J. G. Riess, M. Postel, *Biomater. Artif. Cells Immobilization Biotechnol.* **1992**, *20*, 819–830; b) M. G. Freire, A. M. A. Dias, M. A. Z. Coelho, J. A. P. Coutinho, I. M. Marrucho, *J. Colloid Interface Sci.* **2005**, *286*, 224–232.
- [7] J. L. Vivero-Escoto, R. C. Huxford-Phillips, W. Lin, *Chem. Soc. Rev.* **2012**, *41*, 2673–2685.
- [8] S. Watanabe, H. Oaki, K. Mitsunashi, S. Nakahara, *Makromol. Chem.* **1992**, *193*, 2781–2792.
- [9] S. Wang, M. Zhang, D. Wang, S. Liu, *Microporous Mesoporous Mater.* **2011**, *139*, 1–7.
- [10] S. Mizukami, S. Watanabe, Y. Hori, K. Kikuchi, *J. Am. Chem. Soc.* **2009**, *131*, 5016–5017.
- [11] S. H. Roy, *Int. J. Radiat. Oncol. Biol. Phys.* **2004**, *59*, 21–26.
- [12] Y. Matsumura, H. Maeda, *Cancer Res.* **1986**, *46*, 6387–6392.
- [13] S. Li, L. Huang, *Biochim. Biophys. Acta Biomembr.* **2009**, *1788*, 2259–2266.
- [14] D. Peters, M. Kastantin, V. R. Kotamraju, P. P. Karmali, K. Gujraty, M. Tirrell, E. Ruoslahti, *Proc. Natl. Acad. Sci. USA* **2009**, *106*, 9815–9819.
- [15] C. Clementi, K. Miller, A. Mero, R. Satchi-Fainaro, G. Pasut, *Mol. Pharm.* **2011**, *8*, 1063–1072.